

## WASP-4 is Accelerating Towards the Earth

L. G. BOUMA,<sup>1</sup> J. N. WINN,<sup>1</sup> A. W. HOWARD,<sup>2</sup> S. B. HOWELL,<sup>3</sup> H. ISAACSON,<sup>4</sup> H. KNUTSON,<sup>5</sup> AND R. A. MATSON<sup>3</sup>

<sup>1</sup> *Department of Astrophysical Sciences, Princeton University, 4 Ivy Lane, Princeton, NJ 08540, USA*

<sup>2</sup> *Cahill Center for Astrophysics, California Institute of Technology, Pasadena, CA 91125, USA*

<sup>3</sup> *NASA Ames Research Center, Moffett Field, CA 94035, USA*

<sup>4</sup> *Astronomy Department, University of California, Berkeley, CA 94720, USA*

<sup>5</sup> *Division of Geological and Planetary Sciences, California Institute of Technology, Pasadena, CA 91125, USA*

(Received February 3, 2020; Revised —; Accepted —)

Submitted to AAS journals.

### ABSTRACT

Space and ground-based transit measurements of the hot Jupiter WASP-4b have recently shown that its orbital period appears to be decreasing. Proposed explanations for the period change include tidal orbital decay, orbital precession, and light-travel time effects. We present new radial velocity measurements of WASP-4, acquired with Keck-HIRES. The data show that the system is accelerating towards the Earth at  $\dot{\gamma} = -0.0422_{-0.0027}^{+0.0028} \text{ m s}^{-1} \text{ day}^{-1}$ . The implied period decrease explains most or all of WASP-4’s changing orbital period as a light-travel time effect ( $-5.94 \pm 0.39 \text{ msec yr}^{-1}$  implied, compared to  $-8.64 \pm 1.26 \text{ msec yr}^{-1}$  observed). Combining the radial velocities with new upper limits from speckle imaging, we find that the system’s acceleration is likely caused by a  $10\text{--}200 M_{\text{Jup}}$  companion with semi-major axis between 10–100 AU. The statistics from Knutson et al. (2014) imply that about 1 in 6 hot Jupiters are expected to show period decreases comparable to WASP-4, due to acceleration by outer companions. These period changes will be increasingly measureable in coming years, because the precision of the period derivative measurement scales with the observing baseline to the power of 5/2. Continued radial velocity monitoring of hot Jupiters is therefore essential to distinguish tidal orbital decay from line-of-sight accelerations.

**Keywords:** Exoplanet tides (497), Exoplanet dynamics (490), Radial velocity (1332), Transit timing variation method (1710)

### 1. INTRODUCTION

The orbits of most hot Jupiters are unstable to tidal decay (Counselman 1973; Hut 1980; Rasio et al. 1996; Levrad et al. 2009; Matsumura et al. 2010). The relevant issue is whether the timescale for tidal orbital decay is shorter or longer than the timescale for main-sequence stellar evolution. This question depends on the uncertain rate at which friction inside the star can damp the energy of tidal oscillations and thereby shrink the orbit (as reviewed by Mazeh 2008 and Ogilvie 2014).

Indirect studies of age and angular momentum indicators including the hot Jupiter semi-major axis distribution, host star spin rates, and galactic velocity dispersions have led to estimates for the inspiral timescale that vary from much less to much greater than the main-sequence evolution time (e.g., Jackson et al. 2009, Teitler & Königl 2014, Penev et al. 2018,

Collier Cameron & Jardine 2018, Hamer & Schlaufman 2019). Direct measurements of tidal orbital decay through transit and occultation timing could provide an empirical resolution. For instance, combined transit timing and radial velocity measurements for WASP-12b have shown that its secular period decrease of  $\approx 30$  milliseconds per year is probably due to tidal orbital decay (Maciejewski et al. 2016; Patra et al. 2017; Yee et al. 2020).

This study highlights a point that, though obvious, has perhaps not yet received due attention. The point is that observational programs aimed at identifying orbital decay in hot Jupiters through transit timing will be crippled without concurrent long-term radial velocity monitoring. The reason is that line-of-sight accelerations due to outer companions (e.g., Agol et al. 2005) and tidal orbital decay both initially manifest identically in transit times, as a non-zero period derivative. Massive outer companions to hot Jupiters are the norm; Bryan et al. (2016) calculated an occurrence rate of  $60.9_{-5.6}^{+5.2}\%$  for outer companions to hot Jupiters with masses from  $1\text{--}20 M_{\text{Jup}}$  and semi-major axes from 5–100 AU. Therefore it could very well be that more hot Jupiters will show

shrinking orbital periods due to long term accelerations than due to tidal orbital decay.

The main focus of this study is the hot Jupiter WASP-4b, which has an orbital period that appears to be decreasing by about 10 milliseconds per year. We discovered the timing variations by combining data from TESS (Ricker et al. 2015) with a decade of ground-based observations (Bouma et al. 2019, hereafter B19). Thereafter, Southworth et al. (2019) reported 22 new transit times for the system, and found an updated decay rate of  $\dot{P} = -9.2 \pm 1.1$  milliseconds per year. The Southworth et al. decay rate was  $\approx 3\sigma$  less rapid than that found by B19, but the conclusions of the studies were otherwise similar. A separate study by Baluev et al. (2019) reported additional archival transit light curves of WASP-4b from TRAPPIST and select other observers. Baluev et al. (2019) pointed out that when using lower-precision subsets of the available transit data, the case for a decreasing period worsened.

To determine the origin of the period change, we acquired four additional radial velocity measurements using Keck-HIRES, extending the RV baseline from 3 to 9 years. Previously, the five available HIRES radial velocities suggested a weak ( $\approx 2\sigma$ ) linear trend (Knutson et al. 2014). Our new measurements reveal a line-of-sight acceleration of  $\dot{\gamma} = -0.0422^{+0.0028}_{-0.0027} \text{ ms}^{-1} \text{ day}^{-1}$ . This translates to an expected period decrease from the light-travel time effect of -5.9 milliseconds per year—about commensurate with what is observed from transits. While the apparent period change caused by a line-of-sight acceleration has been referred to as the “Rømer effect” (Yee et al. 2020), we prefer to avoid this term, which typically signifies arrival time delay due to observatory motion. We are discussing the Doppler effect seen by a stationary observer for a source with constant line-of-sight acceleration.

In the following, Section 2 collects the available transit data and presents the new radial velocity and speckle imaging observations. Section 3 analyzes the data, and finds that they yield a picture in which the WASP-4 system is accelerating towards our line-of-sight, likely due to the pull of a brown or M-dwarf companion. Section 4 places this result in the broader context of orbital decay searches, and points out that line-of-sight accelerations, *i.e.*, “false positive orbital decay signals”, are relatively common in the hot Jupiter population. Section 5 offers concluding remarks.

## 2. OBSERVATIONS

### 2.1. Transits

Table 1 lists the transit times we collected for our analysis. We include data from the peer-reviewed literature for which (i) the analysis was based on observations of a single transit, (ii) the midpoint was fitted as a free parameter, and (iii) the time system specified both the leap second correction (TDB or UTC) and also whether any barycentric or heliocentric corrections had been performed.

The majority of times are identical to those we collected in B19. Twenty-two new times reported by Southworth et al. (2019) are included. These transits were observed from the

3.58m NTT and Danish 1.54m telescopes at La Silla, and the SAAO 1.0m telescope.

Additional timing measurements were also recently made available by Baluev et al. (2019), based on a homogeneous analysis of archival ground-based observations. We included twelve of their “high quality” transit times from TRAPPIST (six transits), El Sauce (four transits), and Petrucci et al. (2013). For TRAPPIST and El Sauce, we verified with the original observers that correct barycentric and leap-second corrections had been performed (M. Gillon, P. Evans, priv. comm.). We omitted the fourteen remaining Baluev et al. ETD<sup>1</sup> times due to ambiguity in whether leap-second corrections had or had not been performed.

The four available occultations tabulated by B19 have negligible statistical value due to their large uncertainties, and we forgo their use in this analysis.

### 2.2. Radial velocities

After identifying the period decrease in B19, we acquired four additional radial velocity measurements with the Keck High Resolution Echelle Spectrometer (HIRES; Vogt et al. 1994). Our observations were acquired using the standard setup and reduction techniques of the California Planet Survey (Howard et al. 2010). Previously, the HIRES data-points spanned 2010 to 2013 (Knutson et al. 2014). Our new measurements triple the HIRES observing baseline to nine years.

The complete set of radial velocity observations is given in Table 2. Along with the 2010-2019 HIRES observations, there are also measurements from CORALIE and HARPS. Following B19, we included the CORALIE measurements from Wilson et al. (2008) and Triaud et al. (2010), using the homogeneous values calculated by the latter authors.

For HARPS, we included the values reported by Pont et al. (2011) and Husnoo et al. (2012). While Triaud et al. (2010) also acquired HARPS data over three nights for Rossiter-McLaughlin observations, these data were reduced with a non-standard pipeline, and so are systematically offset from the remaining HARPS data. In our final fit, we therefore omitted the three Triaud et al. (2010) nights. We did nonetheless experiment with using the recent Trifonov et al. (2020) re-reductions, which allowed us to include two calibration RVs taken as part of the Triaud et al. (2010) program. The decision regarding whether to include or omit these points did not noticeably affect our results.

### 2.3. Speckle imaging

An initial analysis of the new HIRES observations led to our detection of a linear trend in the residuals after fitting out the orbit of WASP-4b. This prompted us to acquire speckle images using Zorro at Gemini-South (see Scott et al. 2018, and the instrument web-pages<sup>2</sup>). Zorro is a dual-channel speckle interferometer employing narrow-band filters centered at 562 nm and 832 nm.

<sup>1</sup> <http://var2.astro.cz/ETD>

<sup>2</sup> [www.gemini.edu/sciops/instruments/alopeke-zorro/](http://www.gemini.edu/sciops/instruments/alopeke-zorro/)

We observed WASP-4 twice, on the night of September 11-12 with relatively poor seeing ( $1.2''$ ) and also on the night of September 28-29. Over each observation, we acquired three sets of 1000 60msec exposures. If a companion is present, the autocorrelation functions of these speckle images reveal a characteristic interference pattern. This pattern is then used to determine the properties of the detected companion and to produce a reconstructed image. Using the reconstructed speckle images, contrast curves are produced yielding 5-sigma detection limits (see [Howell et al. 2011](#)). No companions were detected, and the second night, which had better seeing ( $0.6''$ ), also produced the more constraining result. The 832nm limits were the most useful to us given that faint companions are redder than the host star. We therefore opted to use the 832nm September 28-29 contrast limits for the remaining analysis.

### 3. ANALYSIS

#### 3.1. Transits

We considered two models for the observed transit times. The first model assumes a constant orbital period  $P$  on a circular orbit:

$$t_{\text{tra}}(E) = t_0 + PE, \quad (1)$$

where  $E$  is the integer transit number and  $t_0$  is a reference epoch. The second model assumes that the period changes at a steady rate:

$$t_{\text{tra}}(E) = t_0 + PE + \frac{1}{2} \frac{dP}{dE} E^2. \quad (2)$$

The free parameters are the reference epoch  $t_0$ , the period at the reference epoch  $P$ , and the period derivative,  $dP/dt = (1/P)dP/dE$ . We defined the epoch numbers such that  $E = 0$  is near the weighted average of the observed times. This helps to reduce the covariance between  $t_0$  and  $P$ . A third possible model that we did not consider for reasons that will become apparent is a precessing, eccentric orbit (e.g., [Giménez & Bastero 1995](#); [Patra et al. 2017](#)).

We fitted each model by assuming a Gaussian likelihood and sampling over the posterior probability distributions. We sampled the posterior using the algorithm proposed by [Goodman & Weare \(2010\)](#) and implemented by [Foreman-Mackey et al. \(2013\)](#) in `emcee`. The prior for the quadratic model allowed the period derivative to have any sign.

Figure 1 shows the observed transit times, minus the best-fit constant period model. The best-fitting constant-period model has 91 degrees of freedom,  $\chi^2 = 276$ , and  $\chi_{\text{red}}^2 = 3.0$ . The best-fitting quadratic model has 90 degrees of freedom,  $\chi^2 = 183$ , and  $\chi_{\text{red}}^2 = 2.0$ . The difference in the Bayesian information criteria (BIC) between the linear and quadratic and models is  $\Delta\text{BIC} = 89$ , strongly favoring the quadratic model ([Kass & Raftery 1995](#)).

From the reduced  $\chi^2$  values, we can surmise that neither model entirely describes the transit data—there must be some additional source of signal or noise. In [B19](#), we found that the quadratic model for the (sparser) transit data gave  $\chi_{\text{red}}^2 = 1.0$ .

The worsened  $\chi_{\text{red}}^2$  could reflect underestimated statistical uncertainties in any of our transit measurements. It could also reflect systematic errors in the time-systems in which the transit measurements were recorded, though we have taken every caution against this latter possibility.

One approach to analyzing such data would be to inflate the transit measurement uncertainties, and lower the reduced  $\chi^2$ . We do not think that such an approach is warranted, because it would not change the result that the quadratic model is strongly preferred. Instead, we opt to simply inflate the uncertainties reported for each model by a factor of  $(\chi_{\text{red}}^2)^{1/2}$ , or  $\approx 1.73\times$  for the linear model, and  $\approx 1.41\times$  for the quadratic.

The resulting best-fit period derivative for the quadratic model is

$$\dot{P} = -(2.74 \pm 0.28) \times 10^{-10} = -8.64 \pm 1.26 \text{ msec yr}^{-1}. \quad (3)$$

This agrees to within  $1\sigma$  of the value reported by [Southworth et al. \(2019\)](#) ( $\dot{P} = -9.2 \pm 1.1 \text{ ms yr}^{-1}$ ). It is  $\approx 2.3\sigma$  larger than the rate of period decrease we previously reported ( $-12.6 \pm 1.2 \text{ ms yr}^{-1}$ ; [B19](#)), presumably because of the new data from [Southworth et al.](#) and [Baluev et al.](#) The other best-fit transit timing model parameters are reported in Table 3.

#### 3.2. Radial velocities

Our initial model for the radial velocity data was a single Keplerian orbit, plus instrument offsets, jitters, and a long-term linear trend ([Fulton et al. 2018](#), `radvel`). We set Gaussian priors on the orbital period and time of inferior conjunction using the values from Table 4 of [B19](#), and fixed WASP-4b's eccentricity to zero ([Beer et al. 2011](#); [Knutson et al. 2014](#); [Bonomo et al. 2017](#)). The free parameters were the velocity semi-amplitude, the instrument zero-points, an additive “white noise” instrument jitter for each instrument, and a linear ( $\dot{v}_r$ ) acceleration term. We also considered a model without the linear trend, and found that it was disfavored by  $\Delta\text{BIC} = 73$ .

In the preferred “planet+linear trend” model, WASP-4 is accelerating towards our line-of-sight at high confidence,

$$\dot{v}_r = \dot{\gamma} = -0.0422^{+0.0028}_{-0.0027} \text{ m s}^{-1} \text{ day}^{-1}. \quad (4)$$

The remaining radial velocity model parameters are listed in Table 4. For comparison, before our new measurements,  $\dot{\gamma}$  was thought to be about five times smaller, and had marginal statistical significance ([Knutson et al. 2014](#); [Bouma et al. 2019](#)).

The system's acceleration towards our line-of-sight causes a decrease in the apparent orbital period:

$$\dot{P}_{\text{RV}} = \frac{\dot{v}_r P}{c}, \quad (5)$$

or in more convenient units,

$$\dot{P}_{\text{RV}} = 105.3 \text{ msec yr}^{-1} \left( \frac{P}{\text{day}} \right) \left( \frac{\dot{\gamma}}{\text{m s}^{-1} \text{ day}^{-1}} \right). \quad (6)$$

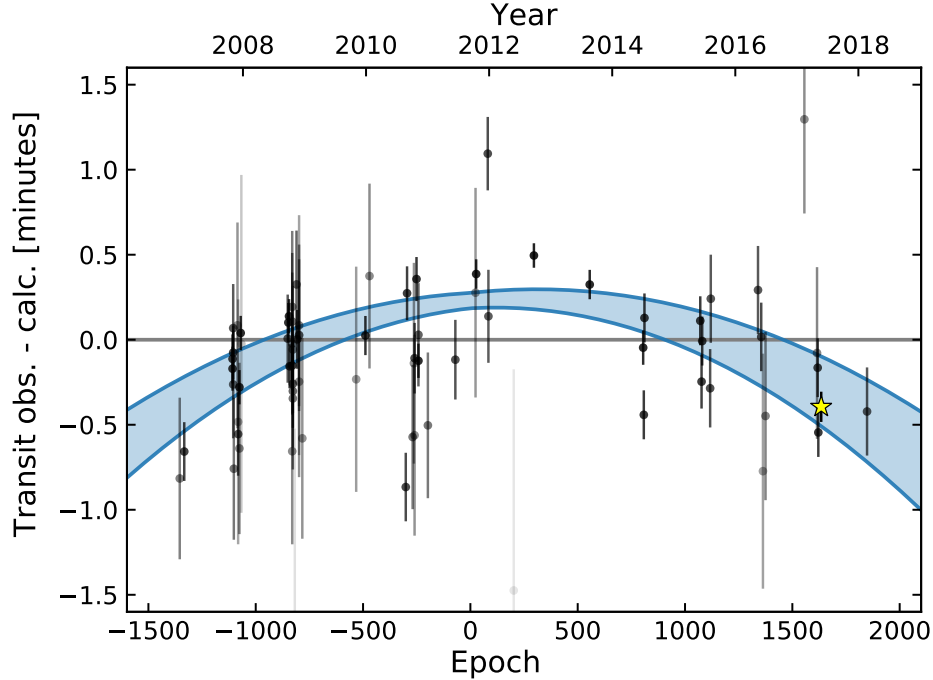


**Figure 1. Timing residuals and best-fit models for WASP-4b.** The vertical axis shows the observed transit times minus the calculated times assuming a constant orbital period. More opaque points correspond to more precise data. The  $\pm 1\sigma$  uncertainties of the quadratic ephemeris are shown in blue. The binned TESS point (yellow star) is the weighted average of 18 TESS transits and is binned for display purposes only. The models were fitted to all of the individual transit times.

For WASP-4, this yields

$$\dot{P}_{\text{RV}} = -5.94 \pm 0.39 \text{ msec yr}^{-1}. \quad (7)$$

The majority of the period decrease seen in transits ( $\dot{P} = -8.64 \pm 1.26 \text{ msec yr}^{-1}$ ) therefore seems to be caused by the acceleration of the host star.

An important consideration is whether the measured RV trend is correlated with stellar activity. We investigate this by analyzing WASP-4’s emission in the Ca II H & K lines, as quantified with the chromospheric  $S$ -index (Wright et al. 2004). We only examined the HIRES velocities for this step, since they are the main source of signal for our analysis. First, we subtracted the orbital solution from the Keck-HIRES velocities. Then, following Bryan et al. (2016, 2019), we calculated the Spearman rank correlation coefficient between the  $S$ -index and the orbit-subtracted velocities. We found a correlation coefficient of 0.16. This correlation is not statistically significant; the corresponding  $p$ -value is 0.65. Furthermore, inspection of the  $S$ -index timeseries did not show secular or sinusoidal trends, as would be expected if we were observing a long-term magnetic activity cycle. The  $S$ -index values are included in Table 2. We conclude that it is highly unlikely that the linear trend is caused by stellar activity.

### 3.3. Constraints on companion masses and semi-major axes

Given a linear radial velocity trend, we can place lower-limits on the mass and semi-major axis of additional bodies in the system. For a quick estimate of the minimum mass

required to explain the linear trend in WASP-4, we turn to Feng et al. (2015). As they discuss, the scenario that yields the minimum companion mass for a system with a linear trend is a companion with  $e \approx 0.5$  and  $\omega = 90^\circ$ . Substituting  $P \approx 1.25\tau$  and  $K \approx 0.5\tau\dot{\gamma}$  into the mass function (e.g., Wright & Howard 2009) yields

$$M_{\text{min}} \approx 5.99 M_{\text{Jup}} \left( \frac{\tau}{\text{yr}} \right)^{4/3} \left| \frac{\dot{\gamma}}{\text{ms}^{-1} \text{ day}^{-1}} \right| \left( \frac{M_{\star}}{M_{\odot}} \right)^{2/3}, \quad (8)$$

where  $\tau$  is the observing baseline. For WASP-4, this gives  $M_{\text{min}} = 4.9 M_{\text{Jup}}$ . Higher masses are allowed for companions that orbit further from the star: at fixed  $\dot{\gamma}$ ,  $M_{\text{comp}} \propto a^2$  (Torres 1999; Liu et al. 2002).

High-resolution images can further limit the available parameter space by setting an upper limit on the semimajor axis, and a maximum brightness (and thereby mass) of any putative companions. The procedure we use to combine constraints from both radial velocities and high resolution imaging has been developed by Wright et al. (2007), Crepp et al. (2012), Montet et al. (2014), Knutson et al. (2014), Bryan et al. (2016, 2019), and others.

*Speckle imaging constraints*—First, we would like to convert the contrast ratios obtained through the Zorro imaging (Figure 3) to limits on the masses of putative companions and their separations from the host star.

To do this, we followed Montet et al. (2014), and opted to employ the Baraffe et al. (2003) models for substellar mass objects and the MIST isochrones for stellar mass objects (Paxton et al. 2011, 2013, 2015; Dotter 2016; Choi et al.

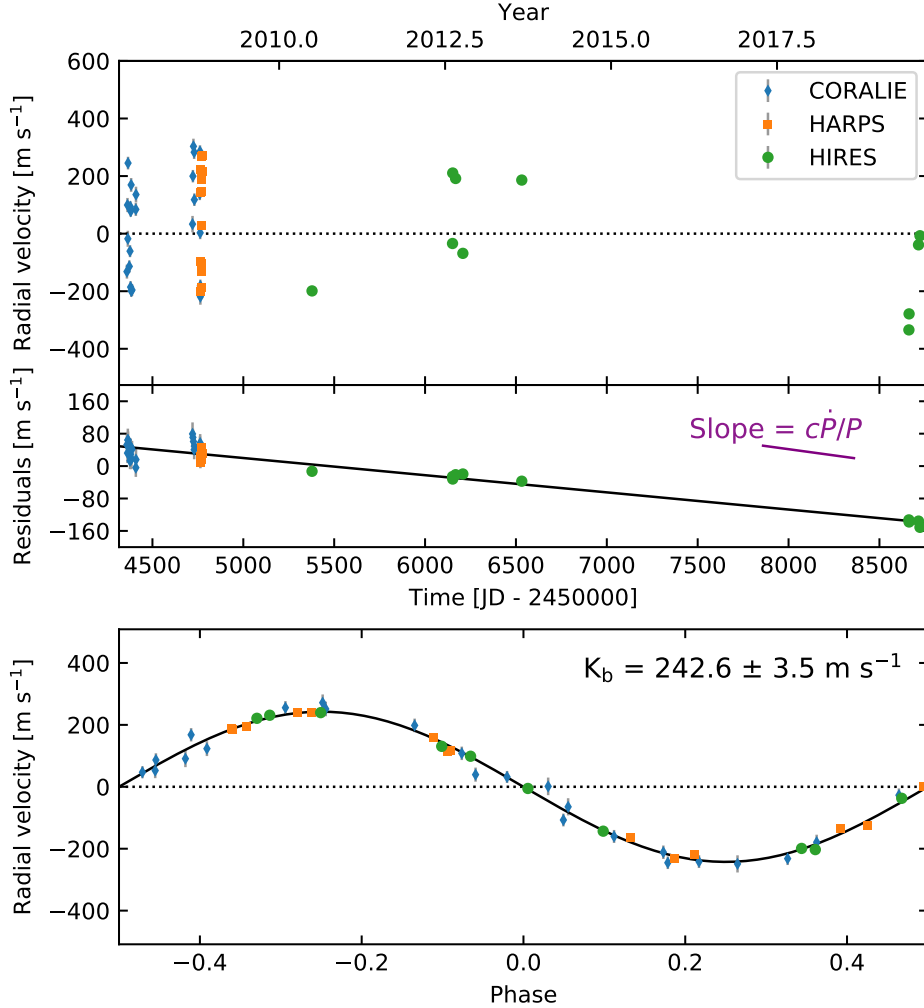


**Figure 2. Radial velocities of WASP-4.** *Top:* RV measurements, with best-fit instrument offsets added. *Middle:* Residuals, after subtracting the maximum-likelihood orbit of WASP-4b. The linear trend inferred from the RV data is shown with a black line. The trend that would be needed to produce the period decrease seen in transits ( $\dot{P} = -8.64 \pm 1.26 \text{ msec yr}^{-1}$ ) is indicated in purple. The four new RV measurements from this work increase the significance of the linear trend from  $\approx 2\sigma$  to  $15\sigma$ . *Bottom:* Phased orbit of WASP-4b.

2016). We assumed that the system age was 5 Gyr, so that companions would have fully contracted.

Due to the custom filters of the Zorro imager, and corresponding lack of synthetic photometry, we further assumed that all sources had blackbody spectra. While this is a simplification, we do not readily have access to the planetary and stellar atmosphere models needed for the consistent calculation with the COND03 and MESA models. We therefore adopted the effective temperatures and bolometric luminosities from the Baraffe et al. (2003) and MIST isochrones. Using these theoretical quantities and the empirically-measured Zorro bandpasses, we calculated absolute magnitudes in the 562 and 832 nm Zorro bands for stellar and planetary mass companions. Applying the same calculation to WASP-4 itself using the effective temperature and bolometric luminosity from B19, we derived the transformation from contrast ratio to companion mass. The resulting limits are shown in Figure 4.

*Radial velocity constraints*—To derive constraints on possible companion masses and separations from the radial velocities, we mostly followed the procedure of Bryan et al. (2019).

We began by defining a  $128 \times 128$  grid in true planetary mass and semimajor axis, with even logarithmic spacing from 1 to  $900 M_{\text{Jup}}$  and 3 to 500 AU. We then considered the possibility that an additional companion in any particular cell could explain the observed linear trend. In each cell, we simulated 512 hypothetical companions.

We assigned each companion a mass and semimajor axis from log-uniform distributions within the grid cell. We drew the inclination from a uniform distribution in  $\cos i$ . For companion masses less than  $10 M_{\text{Jup}}$ , we drew the eccentricity from Kipping (2013)’s long-period exoplanet Beta distribution ( $a = 1.12$ ,  $b = 3.09$ ). If the companion mass exceeded  $10 M_{\text{Jup}}$ , we drew the eccentricity from the power-law  $p_e \propto e^\eta$  reported by Moe & Di Stefano (2017) in their Equation 17 ( $\eta \approx 0.5$  for most orbital periods). The long-period exo-



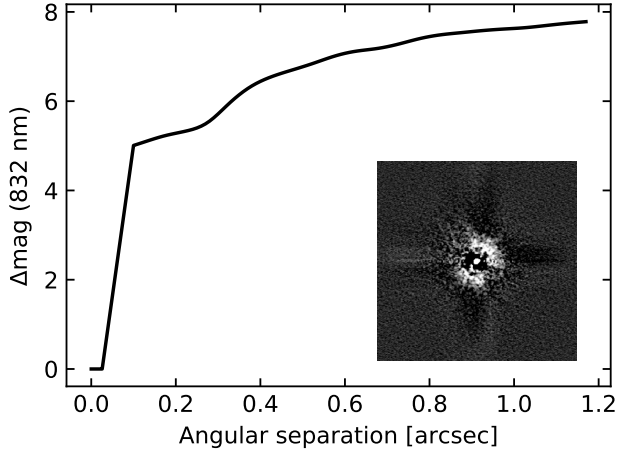


**Figure 3. Zorro contrast limits derived from point-source injection-recovery experiments.** Sources below the curve would have been detected. The inset shows the speckle image reconstructed from 1000 60 millisecond frames in an 832nm bandpass, and acquired on September 28, 2019. The image scale is  $2.46'' \times 2.46''$ .

planet and long-period binary eccentricity distributions are quite different: the exoplanet distribution is “bottom-heavy”, with eccentricities preferentially close to zero. The binary star distribution is “top-heavy”, with eccentricities closer to one. We chose a mass cutoff of  $10M_{\text{Jup}}$  to separate the two regimes based on the bound observed by [Schlaufman \(2018\)](#) between giant planets and brown dwarfs, though this value is also close to the  $13M_{\text{Jup}}$  deuterium-burning limit (e.g., [Burrows et al. 1997](#)).

For each simulated companion, we then drew a sample from the converged chains of our initial model of WASP-4b. We subtracted the planet’s orbital solution, leaving RV points with a linear trend. Given  $(a_c, M_c, e_c)$  for each simulated outer companion, and the fixed instrument offsets and jitters from the MCMC chains, we then performed a maximum likelihood fit for the time and argument of periastron of the outer simulated companion. We converted the resulting  $128 \times 128 \times 512$  cube of log-likelihood values to probabilities, and averaged over the samples in each grid cell to derive a probability distribution in mass and semi-major axis. Figure 4 shows the result.

## 4. DISCUSSION

### 4.1. Implications for WASP-4

Previous potential explanations for WASP-4b’s decreasing orbital period included tidal orbital decay, orbital precession, and light-travel time effects ([Bouma et al. 2019](#)). Our new radial velocity measurements strongly indicate that the least exotic option—light-travel time effects—is also the most likely. Transits show the orbital period decreasing by  $-8.64 \pm 1.26 \text{ ms yr}^{-1}$ ; the line-of-sight acceleration observed in radial velocities would predict a period decrease of  $-5.94 \pm 0.39 \text{ ms yr}^{-1}$ . Though the quantitative agreement is  $\approx 2\sigma$  discrepant, Occam’s razor would suggest that most or

all of the apparent decrease of WASP-4b’s orbital period is caused by the line-of-sight acceleration.

The corresponding requirements for the companion causing the acceleration are that it is likely either a brown-dwarf or low mass star, orbiting between 10-100 AU from the host star (Figure 4). Given such a mass, this companion could at one time have influenced the orbital evolution of the inner giant. The fact that most hot Jupiters have similar massive outer companions ([Knutson et al. 2014](#); [Bryan et al. 2016](#)) is circumstantial evidence for certain high-eccentricity formation pathways (see [Dawson & Johnson 2018](#)). Further radial velocity monitoring should eventually reveal the orbital parameters and minimum mass of WASP-4’s companion.

### 4.2. How many other hot Jupiters are accelerating towards the Earth?

We identified WASP-4b’s decreasing orbital period as part of a search for tidal orbital decay. However, most hot Jupiters have companions outside of 5 AU with super-Jovian masses ([Knutson et al. 2014](#); [Bryan et al. 2016](#)). Line-of-sight accelerations are correspondingly common in hot Jupiter systems.

To evaluate the importance of these effects for future transit timing analyses, we collected the linear radial velocity trends reported by [Knutson et al. \(2014\)](#), and computed the expected orbital period derivatives  $\dot{P}_{\text{RV}} = \dot{v}_r P / c$  for each system. The results are given in Table 5, and visualized for hot Jupiters with significant ( $>3\sigma$ ) linear trends in Figure 5.

Including WASP-4b, 16 of 51 hot Jupiters surveyed by [Knutson et al. \(2014\)](#) show a non-zero radial velocity trend. Therefore around 1 in 3 hot Jupiters is expected to show period changes commensurate with WASP-4 due to acceleration by outer companions. Half of these will be period decreases<sup>3</sup>, and will be an astrophysical false positive in searches for tidal orbital decay.

### 4.3. At what rate is the measurement precision of $dP/dt$ increasing?

For hot Jupiters that have been monitored over baselines exceeding 10 years, secular changes in their orbital periods are currently being constrained to a precision of  $\lesssim 10 \text{ msec yr}^{-1}$  (e.g., [K. Patra et al. 2020, submitted](#)). This is roughly commensurate with the level of signal many outer companions are expected to induce (Figure 5).

It is therefore pertinent to ask at what point in time further detections of the light-travel time effect will become routine for hot Jupiters. This question is the same as asking: at what rate does the uncertainty in the quadratic term of Equation 2 scale with the observing baseline? We take a Fisher analysis approach to the problem. First, we rewrite Equation 2 as

$$t_{\text{tra}} = a_0 + a_1 E + a_2 E^2, \quad (9)$$

<sup>3</sup> At a population level, one would expect half of the line-of-sight accelerations to be positive, and half negative. Tidal orbital decay however is usually negative, and could eventually manifest as an asymmetry in the  $\dot{P}$  distribution of hot Jupiters.

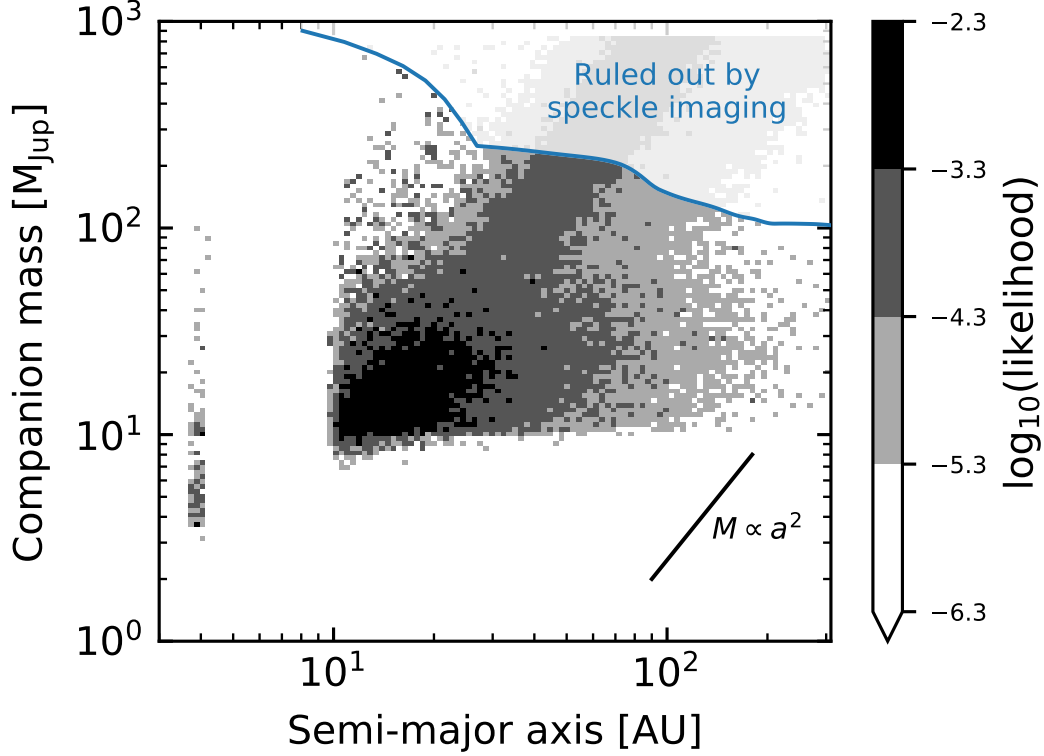


**Figure 4. Masses and semi-major axes of companions that meet requirements of both the radial velocities and the speckle imaging.** The likelihood inferred from radial velocities is shown in grayscale, and the region excluded from the speckle imaging is indicated. The expected mass to semimajor-axis degeneracy is shown with a black line.

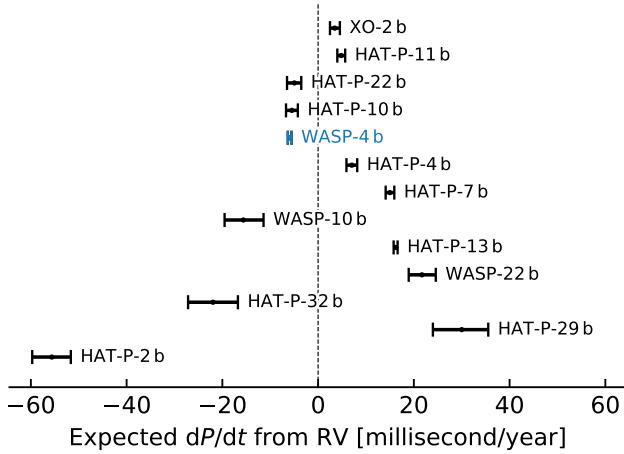


**Figure 5. Predicted hot Jupiter period changes from linear radial velocity trends.** Including WASP-4b, 16 of 51 hot Jupiters from Knutson et al. (2014) have shown long-term radial velocity trends. HAT-P-11 is shown, though its signal may be caused by stellar activity. Three hot Jupiters are not shown because their radial velocity curves are better described as quadratic trends in time: HAT-P-17, WASP-8, and WASP-34. Objects are ordered in the y dimension by the absolute value of  $dP/dt$ .

where  $a_0 \equiv t_0$ ,  $a_1 \equiv P$ , and  $a_2 \equiv 0.5 \cdot dP/dt$ . Following Gould (2003), one can show that if  $N$  transit timing

measurements are taken uniformly across a baseline of  $\Delta E$  epochs with constant precision  $\sigma$ , then the uncertainty of the quadratic term is given by

$$\sigma_{a_2} = 6\sqrt{5} \frac{\sigma}{N^{1/2}(\Delta E)^2} \propto (\Delta E)^{-5/2}. \quad (10)$$

This result implies that a doubled observing baseline yields an  $\approx 5.7$ -fold improvement in precision on  $dP/dt$ . If regular observations continue from ground and space-based observatories, period derivatives will be measured with precision exceeding  $1 \text{ msec yr}^{-1}$  within the coming decade.

## 5. CONCLUSIONS

From newly acquired radial velocity measurements, we found that WASP-4 is accelerating towards the Earth at  $\dot{\gamma} = -0.0422^{+0.0028}_{-0.0027} \text{ ms}^{-1} \text{ day}^{-1}$ . The corresponding light-travel time effect predicts a period decrease  $\dot{\gamma}P/c$  of  $-5.94 \pm 0.39 \text{ msec yr}^{-1}$ . The majority of the period decrease observed in transits ( $\dot{P} = -8.64 \pm 1.26 \text{ msec yr}^{-1}$ ) is therefore explained by the acceleration of the host star — not tidal orbital decay, or apsidal precession. The companion causing the acceleration is most likely a brown dwarf or low-mass star with semi-major axis between 10-100 AU.

Most hot Jupiters have outer companions with masses larger than Jupiter beyond 5 AU (Knutson et al. 2014; Bryan et al. 2016). The accelerations and period changes induced by these outer companions will become an increasingly large

nuisance in the hunt for tidal orbital decay as the observational baselines get longer. In particular, the precision with which the period derivative can be measured from transits scales with the baseline duration to the power of 5/2 (Section 4.3), and so within a decade many more hot Jupiters should show orbital period changes due to accelerations from their outer companions. To distinguish this effect from tidal decay, further long-term radial velocity measurements of hot Jupiters are strongly encouraged.

**Software:** [astrobase](#) (Bhatti et al. 2018), [astropy](#) (Astropy Collaboration et al. 2018), [astroquery](#) (Ginsburg et al. 2018), [corner](#) (Foreman-Mackey 2016), [emcee](#) (Foreman-Mackey et al. 2013), [IPython](#) (Pérez & Granger 2007), [matplotlib](#) (Hunter 2007), [MESA](#) (Paxton et al. 2011, 2013, 2015), [numpy](#) (Walt et al. 2011), [pandas](#) (McKinney 2010), [radvel](#) (Fulton et al. 2018), [scipy](#) (Jones et al. 2001).

**Table 1.** WASP-4b transit times.

$t_{\text{tra}}$ [BJD <sub>TDB</sub> ]	$\sigma_{t_{\text{tra}}}$ [days]	Epoch	Time Reference	Observation Reference
2454368.59279	0.00033	-1354	<a href="#">Hoyer et al. (2013)</a>	<a href="#">Wilson et al. (2008)</a>

NOTE— Table 1 is published in its entirety in a machine-readable format. The first row is shown for guidance regarding form and content.  $t_{\text{tra}}$  is the measured transit midtime, and  $\sigma_{t_{\text{tra}}}$  is its  $1\sigma$  uncertainty. “Time Reference” refers to the provenance of the timing measurement, which may differ from the “Observation Reference” in cases for which a homogeneous timing analysis was performed. The [Hoyer et al. 2013](#) BJD<sub>TT</sub> times are equal to BJD<sub>TDB</sub> for our purposes ([Urban & Seidelmann 2012](#)). We omitted the timing measurements from [Southworth et al. \(2009\)](#), since there were technical problems with the computer clock at the time of observation ([Nikolov et al. 2012](#)). The two [Baxter et al. \(in prep\)](#) times were obtained from Spitzer/IRAC transit light curves in the  $3.6\mu\text{m}$  and  $4.5\mu\text{m}$  channels.

**Table 2.** WASP-4b radial velocities.

Time [BJD <sub>TDB</sub> ]	RV [m s <sup>-1</sup> ]	$\sigma_{\text{RV}}$ [m s <sup>-1</sup> ]	S-value	Instrument	Provenance
2454321.12345	42	0.42	0.42	HIRES	<a href="#">Knutson et al. (2014)</a>

NOTE— Table 2 is published in its entirety in a machine-readable format. The first entry is shown for guidance regarding form and content. S-values are reported only for the HIRES measurements.

**Table 3.** Best-fit transit timing model parameters.

Parameter	Median Value (Unc.) <sup>a</sup>
<i>Constant period</i>	
$t_0$ [BJD <sub>TDB</sub> ]	2456180.558712(+24)(-24)
$P$ [days]	1.338231429(+26)(-26)
<i>Constant period derivative</i>	
$t_0$ [BJD <sub>TDB</sub> ]	2456180.558872(+31)(-31)
$P$ [days]	1.338231502(+24)(-24)
$dP/dt$	$-2.74(+40)(-40) \times 10^{-10}$

**Table 4.** Best-fit radial velocity model parameters.

Parameter	Credible Interval	Maximum Likelihood	Units
<i>Modified MCMC Step Parameters</i>			
$P_b$	$1.338231466 \pm 2.3e-08$	1.338231466	day
$T_{\text{conj}_b}$	$2455804.515752^{+2.5e-05}_{-2.4e-05}$	2455804.515752	BJD <sub>TDB</sub>

Table 4 continued



**Table 4** (*continued*)

Parameter	Credible Interval	Maximum Likelihood	Units
$e_b$	$\equiv 0.0$	$\equiv 0.0$	
$\omega_b$	$\equiv 0.0$	$\equiv 0.0$	$^\circ$
$K_b$	$242.6^{+3.6}_{-3.5}$	242.6	$\text{ms}^{-1}$
<i>Orbital Parameters</i>			
$P_b$	$1.338231466 \pm 2.3e-08$	1.338231466	day
$T_{\text{conj}_b}$	$2455804.515752^{+2.5e-05}_{-2.4e-05}$	2455804.515752	$\text{BJD}_{\text{TDB}}$
$e_b$	$\equiv 0.0$	$\equiv 0.0$	
$\omega_b$	$\equiv 0.0$	$\equiv 0.0$	$^\circ$
$K_b$	$242.6^{+3.6}_{-3.5}$	242.6	$\text{ms}^{-1}$
<i>Other Parameters</i>			
$\gamma_{\text{HIRES}}$	$36.4^{+5.8}_{-5.9}$	36.4	$\text{ms}^{-1}$
$\gamma_{\text{HARPS}}$	$-69.9^{+4.2}_{-4.1}$	-70.1	$\text{ms}^{-1}$
$\gamma_{\text{CORALIE}}$	$-39.9^{+5.5}_{-5.2}$	-40.1	$\text{ms}^{-1}$
$\dot{\gamma}$	$-0.0422^{+0.0028}_{-0.0027}$	-0.0424	$\text{ms}^{-1} \text{ day}^{-1}$
$\ddot{\gamma}$	$\equiv 0.0$	$\equiv 0.0$	
$\sigma_{\text{HIRES}}$	$10.8^{+3.7}_{-2.7}$	8.2	$\text{ms}^{-1}$
$\sigma_{\text{HARPS}}$	$13.0^{+3.7}_{-2.6}$	11.5	$\text{ms}^{-1}$
$\sigma_{\text{CORALIE}}$	$13.8^{+6.6}_{-6.7}$	12.9	$\text{ms}^{-1}$

**Table 5.** Predicted hot Jupiter period changes from linear radial velocity trends reported by [Knutson et al. \(2014\)](#).

Planet	$\dot{\gamma}$ [ $\text{ms}^{-1} \text{ yr}^{-1}$ ]	$+\sigma_{\dot{\gamma}}$ [ $\text{ms}^{-1} \text{ yr}^{-1}$ ]	$-\sigma_{\dot{\gamma}}$ [ $\text{ms}^{-1} \text{ yr}^{-1}$ ]	$P$ [days]	$\dot{P}_{\text{RV}}$ [ $\text{ms yr}^{-1}$ ]	$+\sigma_{\dot{P}_{\text{RV}}}$ [ $\text{ms yr}^{-1}$ ]	$-\sigma_{\dot{P}_{\text{RV}}}$ [ $\text{ms yr}^{-1}$ ]	Significant?
HAT-P-2 b	-0.0938	0.0067	0.0069	5.6335158	-55.62	3.97	4.09	1

NOTE— Table 5 is published in its entirety in a machine-readable format. The first entry is shown for guidance regarding form and content. Orbital periods were retrieved from NASA’s Exoplanet Archive. Additional comments regarding non-linear trends and stellar activity are included in the MRT.

## REFERENCES

- Agol, E., Steffen, J., Sari, R., & Clarkson, W. 2005, *MNRAS*, **359**, 567
- Astropy Collaboration, Price-Whelan, A. M., Sipőcz, B. M., et al. 2018, *AJ*, **156**, 123
- Baluev, R. V., Sokov, E. N., Jones, H. R. A., et al. 2019, *MNRAS*, **490**, 1294
- Baraffe, I., Chabrier, G., Barman, T. S., Allard, F., & Hauschildt, P. H. 2003, *A&A*, **402**, 701
- Beer, I. M., Knutson, H. A., Burrows, A., et al. 2011, *ApJ*, **727**, 23
- Bhatti, W., Bouma, L. G., & Wallace, J. 2018, *astrobase*, <https://doi.org/10.5281/zenodo.1469822>
- Bonomo, A. S., Desidera, S., Benatti, S., et al. 2017, *A&A*, **602**, A107
- Bouma, L. G., Winn, J. N., Baxter, C., et al. 2019, *AJ*, **157**, 217
- Bryan, M. L., Knutson, H. A., Lee, E. J., et al. 2019, *AJ*, **157**, 52
- Bryan, M. L., Knutson, H. A., Howard, A. W., et al. 2016, *ApJ*, **821**, 89
- Burrows, A., Marley, M., Hubbard, W. B., et al. 1997, *ApJ*, **491**, 856
- Choi, J., Dotter, A., Conroy, C., et al. 2016, *ApJ*, **823**, 102
- Collier Cameron, A., & Jardine, M. 2018, *MNRAS*, **476**, 2542
- Counselman, C. C. 1973, *ApJ*, **180**, 307
- Crepp, J. R., Johnson, J. A., Howard, A. W., et al. 2012, *ApJ*, **761**, 39
- Dawson, R. I., & Johnson, J. A. 2018, *ARA&A*, **56**, 175
- Dotter, A. 2016, *ApJS*, **222**, 8
- Dragomir, D., Kane, S. R., Pilyavsky, G., et al. 2011, *AJ*, **142**, 115
- Feng, Y. K., Wright, J. T., Nelson, B., et al. 2015, *ApJ*, **800**, 22
- Foreman-Mackey, D. 2016, *The Journal of Open Source Software*, **24**

- Foreman-Mackey, D., Hogg, D. W., Lang, D., & Goodman, J. 2013, *PASP*, **125**, 306
- Fulton, B. J., Petigura, E. A., Blunt, S., & Sinukoff, E. 2018, *PASP*, **130**, 044504
- Gillon, M., Smalley, B., Hebb, L., et al. 2009, *A&A*, **496**, 259
- Giménez, A., & Bastero, M. 1995, *Ap&SS*, **226**, 99
- Ginsburg, A., Sipocz, B., Madhura Parikh, et al. 2018, *Astropy/Astroquery: V0.3.7 Release*
- Goodman, J., & Weare, J. 2010, *Communications in Applied Mathematics and Computational Science*, **5**, 65
- Gould, A. 2003, *arXiv Astrophysics e-prints*, arXiv:astro-ph/0310577
- Hamer, J. H., & Schlafman, K. C. 2019, *AJ*, **158**, 190
- Howard, A. W., Johnson, J. A., Marcy, G. W., et al. 2010, *ApJ*, **721**, 1467
- Howell, S. B., Everett, M. E., Sherry, W., Horch, E., & Ciardi, D. R. 2011, *AJ*, **142**, 19
- Hoyer, S., López-Morales, M., Rojo, P., et al. 2013, *MNRAS*, **434**, 46
- Huitson, C. M., Désert, J.-M., Bean, J. L., et al. 2017, *AJ*, **154**, 95
- Hunter, J. D. 2007, *Computing in Science & Engineering*, **9**, 90
- Husnoo, N., Pont, F., Mazeh, T., et al. 2012, *MNRAS*, **422**, 3151
- Hut, P. 1980, *A&A*, **92**, 167
- Jackson, B., Barnes, R., & Greenberg, R. 2009, *ApJ*, **698**, 1357
- Jones, E., Oliphant, T., Peterson, P., et al. 2001, *Open source scientific tools for Python*
- Kass, R. E., & Raftery, A. E. 1995, *Journal of the American Statistical Association*, **90**, 773
- Kipping, D. M. 2013, *MNRAS*, **434**, L51
- Knutson, H. A., Fulton, B. J., Montet, B. T., et al. 2014, *ApJ*, **785**, 126
- Levrard, B., Winisdoerffer, C., & Chabrier, G. 2009, *ApJ*, **692**, L9
- Liu, M. C., Fischer, D. A., Graham, J. R., et al. 2002, *ApJ*, **571**, 519
- Maciejewski, G., Dimitrov, D., Fernández, M., et al. 2016, *A&A*, **588**, L6
- Matsumura, S., Peale, S. J., & Rasio, F. A. 2010, *ApJ*, **725**, 1995
- Mazeh, T. 2008, in *EAS Publications Series*, Vol. 29, *EAS Publications Series*, ed. M.-J. Goupil & J.-P. Zahn, 1
- McKinney, W. 2010, in *Proceedings of the 9th Python in Science Conference*, ed. S. van der Walt & J. Millman, 51
- Moe, M., & Di Stefano, R. 2017, *ApJS*, **230**, 15
- Montet, B. T., Crepp, J. R., Johnson, J. A., Howard, A. W., & Marcy, G. W. 2014, *ApJ*, **781**, 28
- Nikolov, N., Henning, T., Koppenhoefer, J., et al. 2012, *A&A*, **539**, A159
- Ogilvie, G. I. 2014, *ARA&A*, **52**, 171
- Patra, K. C., Winn, J. N., Holman, M. J., et al. 2017, *AJ*, **154**, 4
- Paxton, B., Bildsten, L., Dotter, A., et al. 2011, *ApJS*, **192**, 3
- Paxton, B., Cantiello, M., Arras, P., et al. 2013, *ApJS*, **208**, 4
- Paxton, B., Marchant, P., Schwab, J., et al. 2015, *ApJS*, **220**, 15
- Penev, K., Bouma, L. G., Winn, J. N., & Hartman, J. D. 2018, *AJ*, **155**, 165
- Pérez, F., & Granger, B. E. 2007, *Computing in Science and Engineering*, **9**, 21
- Petrucchi, R., Jofré, E., Schwartz, M., et al. 2013, *ApJL*, **779**, L23
- Pont, F., Husnoo, N., Mazeh, T., & Fabrycky, D. 2011, *MNRAS*, **414**, 1278
- Ranjan, S., Charbonneau, D., Désert, J.-M., et al. 2014, *ApJ*, **785**, 148
- Rasio, F. A., Tout, C. A., Lubow, S. H., & Livio, M. 1996, *ApJ*, **470**, 1187
- Ricker, G. R., Winn, J. N., Vanderspek, R., et al. 2015, *Journal of Astronomical Telescopes, Instruments, and Systems*, **1**, 014003
- Sanchis-Ojeda, R., Winn, J. N., Holman, M. J., et al. 2011, *ApJ*, **733**, 127
- Schlaufman, K. C. 2018, *ApJ*, **853**, 37
- Scott, N. J., Howell, S. B., Horch, E. P., & Everett, M. E. 2018, *PASP*, **130**, 054502
- Southworth, J., Hinse, T. C., Jørgensen, U. G., et al. 2009, *MNRAS*, **396**, 1023
- Southworth, J., Dominik, M., Jørgensen, U. G., et al. 2019, *MNRAS*, **490**, 4230
- Teitler, S., & Königl, A. 2014, *ApJ*, **786**, 139
- Torres, G. 1999, *PASP*, **111**, 169
- Triana, A. H. M. J., Collier Cameron, A., Queloz, D., et al. 2010, *A&A*, **524**, A25
- Trifonov, T., Tal-Or, L., Zechmeister, M., et al. 2020, *arXiv:2001.05942 [astro-ph]*, arXiv: 2001.05942
- Urban, S., & Seidelmann, P. 2012, *Explanatory Supplement to the Astronomical Almanac* (University Science Books)
- Vogt, S. S., Allen, S. L., Bigelow, B. C., et al. 1994, *SPIE Conference Series*, ed. D. L. Crawford & E. R. Craine, Vol. 2198
- Walt, S. v. d., Colbert, S. C., & Varoquaux, G. 2011, *Computing in Science & Engineering*, **13**, 22
- Wilson, D. M., Gillon, M., Hellier, C., et al. 2008, *ApJL*, **675**, L113
- Winn, J. N., Holman, M. J., Carter, J. A., et al. 2009, *AJ*, **137**, 3826
- Wright, J. T., & Howard, A. W. 2009, *ApJS*, **182**, 205
- Wright, J. T., Marcy, G. W., Butler, R. P., & Vogt, S. S. 2004, *ApJS*, **152**, 261
- Wright, J. T., Marcy, G. W., Fischer, D. A., et al. 2007, *ApJ*, **657**, 533
- Yee, S. W., Winn, J. N., Knutson, H. A., et al. 2020, *ApJL*, **888**, L5